

Reconciling two-component power spectra

Charles L. Rino

Institute for Scientific Research, Boston College, Chestnut Hill, MA, USA

and

Charles S. Carrano

Institute for Scientific Research, Boston College, Chestnut Hill, MA, USA

and

Keith M. Groves

Institute for Scientific Research, Boston College, Chestnut Hill, MA, USA

and

Patrick Roddy

Air Force Research Laboratory, Hanscom Field, Boston, MA, USA

Version: March 31, 2015

Power-law spectra have been used to interpret scintillation data for decades. Two-component power-law spectra were invoked to explain observed equatorial scintillation from VHF to S-Band. Carrano and Rino developed new strong-scatter theoretical results described in a companion IES 2015 paper. The new theoretical results have been used to estimate two-component power-law parameters from multi-frequency intensity scintillation data.

Although two-component power-law structures have been observed in data from both in-situ rocket and satellite probes, published analyses of C/NOFS high-resolution density data have reported only single power-law characteristics for structure scales greater than 100 m. New results reported in this paper show that two-component power-law spectra are present, but they are confined to the most highly disturbed data segments. We reconcile the main body of C/NOFS data with two-component power-law spectra associated with structure strong enough to generate L-band scintillation.

Key Words: Beacon Satellite, Scintillation, Modeling, Numerical Simulation

1. INTRODUCTION

The phenomena collectively referred to as Equatorial Spread F (ESF) evolve from a broad range of scale-dependent ionospheric processes. For the purposes of this study ionospheric structure is divided into large-scale, intermediate-scale, and small-scale regimes. The large-scale regime includes the background ionosphere and the quasi-equilibrium processes that sustain it. The intermediate-scale regime includes the structure associated with the depletions or plumes that characterize ESF. The small-scale regime includes structure in the diffusion range that supports plume-delineating radar backscatter. Partitioning ionospheric processes by scale constrains both spatial and temporal variations. However, over typical measurement intervals, intermediate-scale structure is spatially invariant with statistically

inhomogeneous and homogeneous stochastic components. Statistically homogeneous structure has sufficient regularity to support well-defined averages of spatial Fourier decomposition intensities.

A wavelet-based analysis procedure for data segmentation and subsequent classification was developed and demonstrated using high-resolution data collected by the Air Force Communication/Navigation Outage Forecasting System (C/NOFS) satellite [1]. The following one-dimensional SDF is hypothesized to characterize statistically homogeneous intermediate-scale structure from the smallest resolved wavenumber, $\Delta q = 2\pi/L_s$ where L_s is the segmentation length, to the largest wavenumber $2\pi/\Delta s$ where Δs is the spatial resolution:

$$\varphi(q) = \begin{cases} C_1 q^{-p_1} & q < q_0 \\ C_2 q^{-p_2} & q > q_0 \end{cases} . \quad (1)$$

A classifier identifies segments that have sufficiently well developed structure to be characterized by (1). For the developed segments the classifier estimates the power-law parameters C_1 , p_1 and C_2 , p_2 independently by identifying the two power-law wave number ranges that provide the best overall fit to measured scale spectra. The goodness-of-fit measure is used to identify statistically homogeneous segments. The break wavenumber q_0 for two-component SDFs can be estimated from the relation

$$q_0 = \exp(\ln(C_2) - \ln(C_1)) / (p_2 - p_1) . \quad (2)$$

This paper summarizes intermediate-scale structure characteristics derived from high-resolution C/NOFS data obtained over a 4-year period from 2011 to 2014. The extended results show that two-component power-law spectra characterize the most highly disturbed C/NOFS segments.

2. RECENT C/NOFS INTERMEDIATE SCALE STRUCTURE ANALYSIS

As described in Rino et al., [1] the analysis procedure extracts high-resolution data, which are resampled to a uniform spatial grid. Figure 1 shows an example of highly structured resampled data from year 2011 day 310. The data subtend 18,945 km (1,349,950 samples at 14.03 m). For discrete wavelet transform (DWT) computation the data are mirror extended to 2^{21} samples. Figure 2 shows the DWT intensity. The C/NOFS segmentation retains the resolved structure finer than 8 octaves below the largest scale shown in Figure 2. This produces 80 segments with 16,384-samples from which scale-spectra are computed by averaging the wavelet contributions. The numbers at the top of the plot are centered on the indicated segment location. Well developed ESF structure corresponds scale-spectra intensities in excess of 100 dB.

As in our previous study [2], the segment summary data are first partitioned into data sets that admit spectral classification based on the overall goodness-of-fit measure and those with undeveloped or poor fits to the hypothesized two-component model. In the absence of preselection we expect most of the segments to be unclassifiable. Figures 3, and 4 show the patterns for two years. Different numbers of high-resolution passes were acquired each year with 2012 being the most complete. The integer fraction in the title of each summary figure is the ratio of classifiable and total segments for the year. The left-frame scatter diagrams show the single-component (blue) and two-component (red) p_1 indices versus the turbulent strength C_1 . The single-component category includes spectra that are noise-limited as well

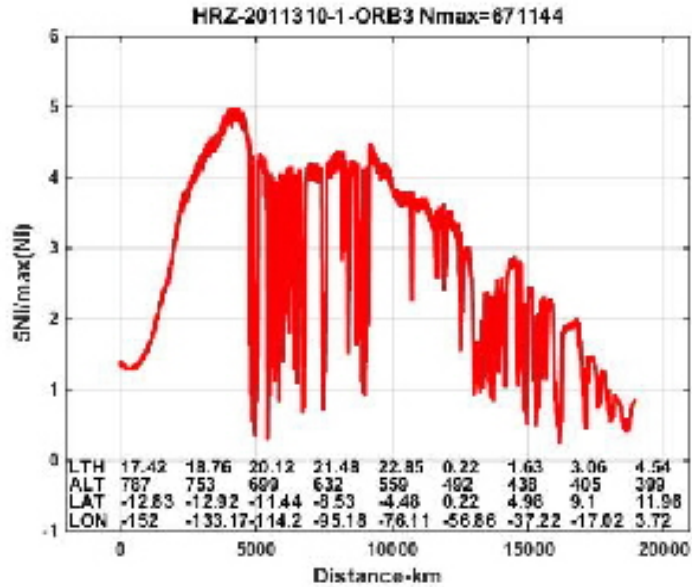


FIG. 1 High resolution C/NOFS data from 2011 day 310 orbit 3. The data have been normalized by $N_{\max} = 6.71144 \times 10^5 \text{ cm}^3$ for display purposes.

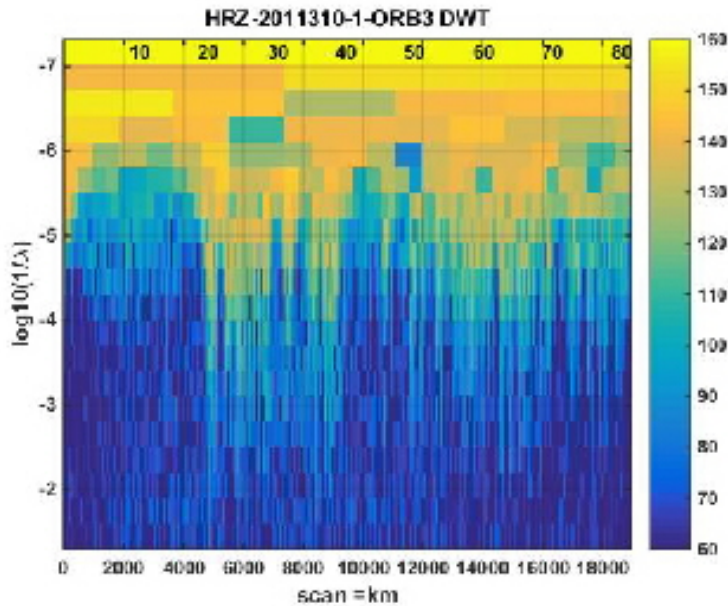


FIG. 2 Discrete wavelet transform of data shown in Figure 1. The wavelet scales span 21 octaves, with 1 through 20 displayed. Numbered segment locations are shown at the top of the display.

as single power-laws that extend into the small-scale diffusion regime. The right-frame histograms summarize the single-component spectral indices. The scale spectra do not have sufficient resolution to capture spectral spectral steepening in the small-scale diffusion regime.

Nearly identical $C1$ versus p_1 patterns are observed over the four-year period. However, the nearly 200 dB range of the reported $C1$ estimates is surprisingly large given that the resolved scale-spectra dB range spans ~ 60 dB. The measured $C1$ values are derived from a log-linear least-squares fit to the large-scale portion of the segment scale spectra. Investigation of the spectra show that substantial variability is characteristic of the large-scale. The well-order $C1$ and p_1 results, particularly at the very low $C1$ levels, support the integrity of the measurement over the full 200 dB range. Indeed, the systematic decrease in p_1 with increasing turbulent strength has been observed in rocket-probe data and in structure characteristics derived from scintillation data as summarized in Rino et al. [1]. The larger data sets show that the trend persists from the largest to the smallest $C1$ values. Scatter in the estimates does increase with increasing turbulence levels. The most probable p_1 value for all single-component power-law segments is larger than 2, but averages over smaller data sets would reflect the particular range of $C1$ values. The smaller reported single-power law described in the previous section are evidently representative of less disturbed segments.

In our previous study we attempted to isolate classifiable individual spectra that fit the ideal model with high confidence. In retrospect, this criterion is too stringent to characterize the two-component structure. In the current analysis all the *classifiable* two-component summary parameters are used. Figures 5 and 6 show the summary results for the two years (2012 and 1013) that provided the largest numbers of segments. The upper frames show the reported p_1 (blue) and p_2 (red) values. The lower frame shows the break scale derived from (2). The scatter is large but the median p_1 values ~ 1.6 and median p_2 values ~ 2.2 with a break scale at ~ 1 km are consistent with parameters derived from analysis of strong-scatter scintillation data. The results also suggest that in such highly disturbed regions spectral characterization itself is more difficult. In this regard, the path-integration to which scintillation responds should mitigate the variation.

3. DISCUSSION

The results of our current analysis show that the most highly disturbed C/NOFS pass segments are characterized by two-component power-law spectra with a transition to a steeper power-law index in the intermediate scale range near one km. The fact that other C/NOFS studies did not report two-component intermediate-scale structure can be attributed to data selection. Multi-instrument coordination constraints make it unlikely that the most highly structured segments are interrogated. Moreover, consistent normalization of the reported spectra to rank the disturbance levels is difficult. However, the propagation disturbance levels that would occur on propagation paths that intercept an extended region of the measured structure levels can be estimated.

A structure model must be introduced to convert measured one-dimensional SDFs to a higher-dimensional structure model. To mesh with the two-dimensional phase-screen theory reported by Carrano and Rino a structure in planes that intercept field lines at near normal incidence is characterized by a two-component model.

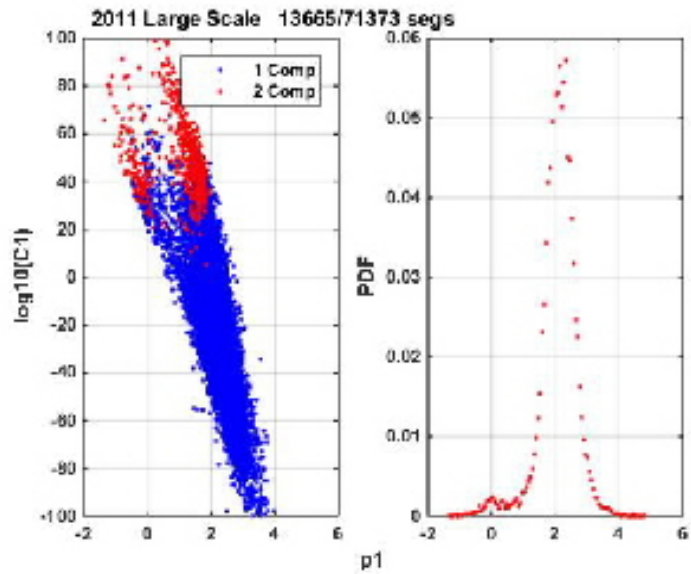


FIG. 3 Summary of classifiable scale-spectra for 2011 segments.

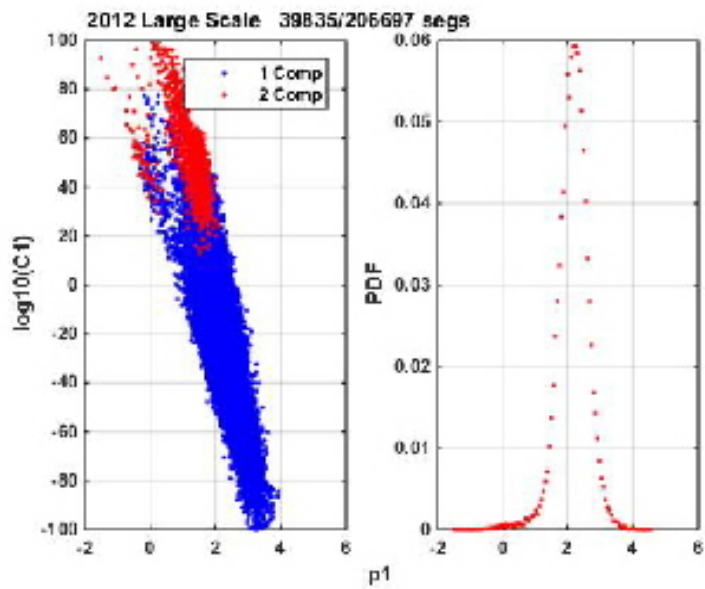


FIG. 4 Summary of classifiable scale-spectra for 2012 segments.

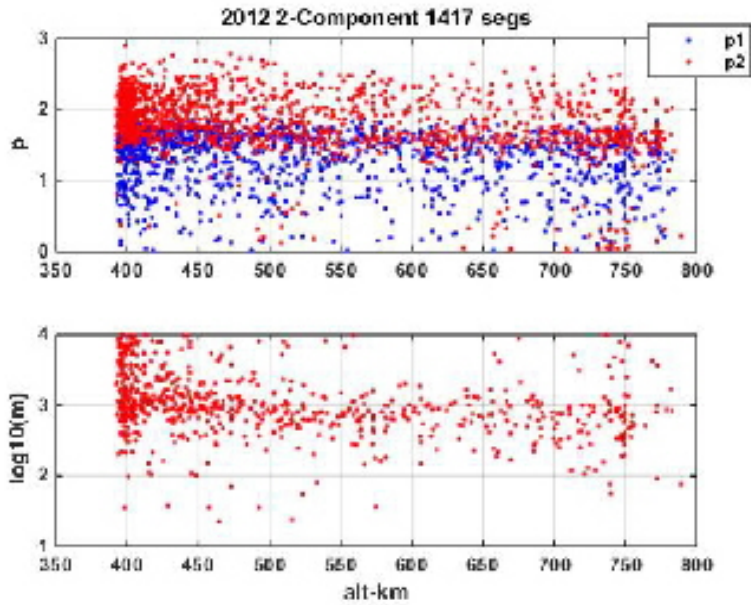


FIG. 5 Summary of year 2012 two-component spectral indices (upper frame) and derived break scale (lower frame).

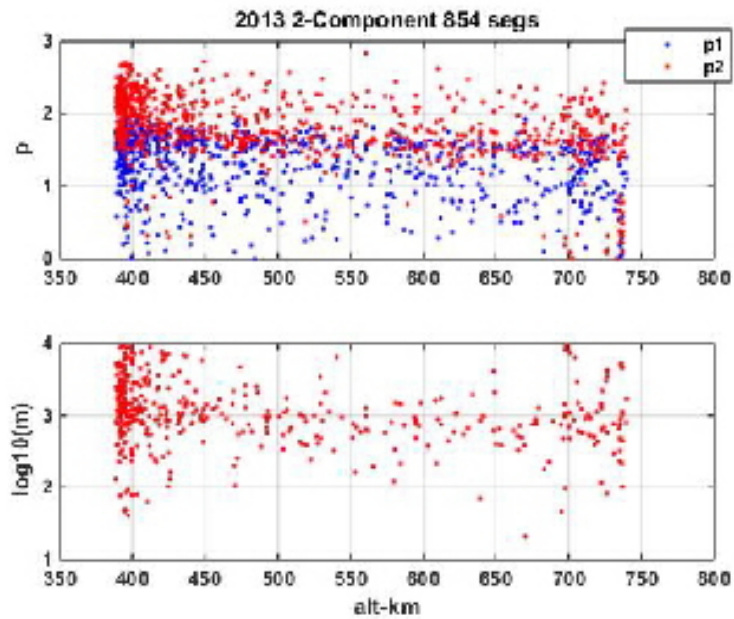


FIG. 6 Summary of year 2013 two-component spectral indices (upper frame) and derived break scale (lower frame).

With some simplifying assumptions the following formula was derived to convert the measured C_1 values to C_s . In consistent units the one-dimensional power-law index in $p_1 = 2v - 1$.

$$C_s = \left[\frac{2\pi^{3/2}\Gamma((p_1 + 1)/2)}{L_s\Gamma(p_1/2)} \right] \Delta s 10^{12} C_1. \quad (3)$$

The corresponding path-integrated phase SDF is

$$\Phi_{\delta\phi}(\kappa) \simeq 4\pi^2 r_e^2 c^2 l_p / f^2 C_s \kappa^{-2v} \quad (4)$$

where f is beacon frequency, l_p is the path length, and L_s , as before, is the segment length. To distinguish between the phase power-law index and the one-dimensional index an overbar will be used for the phase index $\bar{p} = 2v = p + 1$. In the companion paper by Carrano and Rino it is shown that the strong-scatter phase-screen theory is completely defined by the strength parameter

$$U^* = \begin{cases} U_1 & \text{for } q_0 \rho_F \leq 1 \\ U_2 & \text{for } q_0 \rho_F > 1 \end{cases}, \quad (5)$$

where $\mu = q\rho_F$, $U_1 = C_p \rho_F^{\bar{p}_1 - 1}$, $U_2 = C_p q_0^{\bar{p}_2 - \bar{p}_1} \rho_F^{\bar{p}_2 - 1}$, $\rho_F = \sqrt{x/k}$ and

$$C_p = 4\pi^2 r_e^2 c^2 l_p / f^2 C_s. \quad (6)$$

Figure 7 shows the U parameter variation over the C_1 range at 250 MHz (UHF) and 1574 MHz (L1). A path length of 50 km and a 350 km propagation distance were used for the computation. The 50 km path length can be interpreted as a uniform distribution of within a layer or an equivalent length that accommodates strength modulation with no structure change. Varying structure along a propagation path is a topic for further study.

Strong scintillation developed when the U parameter exceeds unity. Thus, strong L1 scintillation is would be expected for the most highly disturbed C/NOFS segments. conditions. Larger U can produce strong L-band focusing where L-band scintillation index exceeds the L-band scintillation index at UHF. GNSS performance is determined by the deep fade occurrence and coherence.

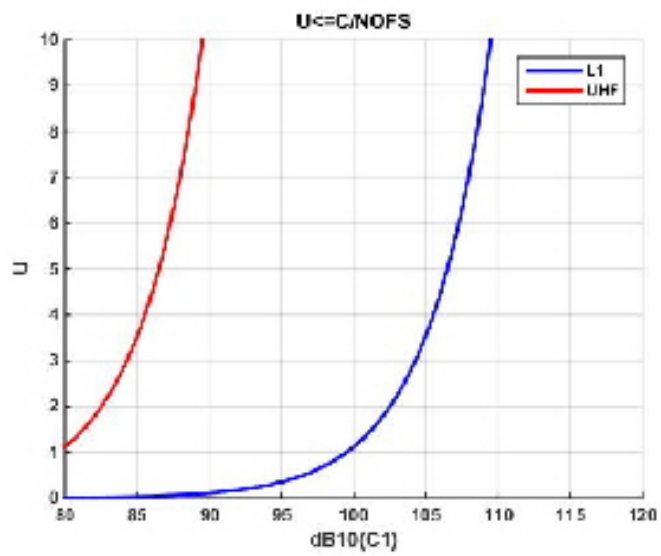


FIG. 7 Estimates of U at UHF and GPS L1 frequencies over an extended $C1$ range.

REFERENCES

- [1] C. L. Rino, C. S. Carrano, and Patrick Roddy. Wavelet-based analysis and power law classification of *c/nofs* high-resolution electron density data. *Radio Science*, 49(doi:10.1002/2013RS005272):680–688, 2014.
- [2] Charles L. Rino and Charles S. Carrano. The application of numerical simulation in beacon scintillation analysis and modeling. *Radio Science*, pages –, 2011.